

Processive bidirectional motion of dynein–dynactin complexes *in vitro*

Jennifer L. Ross¹, Karen Wallace¹, Henry Shuman¹, Yale E. Goldman¹ and Erika L.F. Holzbaur^{1,2}

Cytoplasmic dynein is the primary molecular motor responsible for transport of vesicles, organelles, proteins and RNA cargoes from the periphery of the cell towards the nucleus along the microtubule cytoskeleton of eukaryotic cells. Dynactin, a large multi-subunit activator of dynein, docks cargo to the motor and may enhance dynein processivity. Here, we show that individual fluorescently labelled dynein–dynactin complexes exhibit bidirectional and processive motility towards both the plus and minus ends of microtubules. The dependence of this activity on substrate ATP concentration, nucleotide analogues and inhibitors suggests that bidirectional motility is an active energy-transduction property of dynein–dynactin motor mechano-chemistry. The unique motility characteristics observed may reflect the flexibility of the dynein structure that leads to an enhanced ability to navigate around obstacles in the cell.

Cytoplasmic dynein is a microtubule-activated ATPase that generates force along the microtubule to produce work that transports cargoes in cells. Dynein contains two heavy chains with a molecular weight (M_r) of 512 K and multiple intermediate and light molecular weight subunits¹. The carboxy (C)-terminal two-thirds of the heavy chain folds into a large, planar ring that is comprised of the motor domain, containing six consensus AAA (ATPases with various cellular activities) modules^{2,3}. Four of the modules, AAA1–AAA4, include consensus P-loop motifs that may bind nucleotide³. AAA1 is the primary site of ATP binding and hydrolysis⁴, whereas AAA3 has been shown to increase the activity of dynein by binding, and possibly hydrolysing, ATP^{5,6}.

Dynactin is also a large, multi-subunit complex that is an essential activator of most cytoplasmic dynein functions *in vivo*^{7–9}. An actin-related protein (ARP1) forms a small filament that is the backbone of the complex, and additional subunits cap and stabilize the ARP1 filament. Protruding from the backbone is a dimer of p150^{Glued} subunits that form a coiled coil, and each one ends in a microtubule-binding CAP-Gly (cytoskeletal-associated protein, glycine-rich domain) motif. Dynein intermediate chain binds to the coiled coil of the p150^{Glued} dimer. A mutation in the CAP-Gly domain of the p150^{Glued} subunit of dynactin results in motor neuron degenerative disease^{10,11}. Dynamitin (p50) subunits are localized at the junction of the ARP1 filament with p150^{Glued} to stabilize the connection. Although it has been proposed that dynactin enhances the processivity of dynein by tethering the complex to the microtubule, this hypothesis remains controversial^{12,13}.

Unlike smaller molecular motors¹⁴, dynein's large flexible structure, and modular construction, complicate investigations of energy transduction. Within the dynein motor domain, there is functional coordination

between ATP binding and hydrolysis and the power-stroke. This has only recently been examined by biochemical, structural and single-molecule biophysical experiments^{2,15,16}. Processivity, stall force and step size have been measured in single-molecule studies where dynein was bound to polymer bead cargoes and with mechanical loads applied by an optical trap^{12,16}. As dynactin is required for most dynein-mediated functions in the cell, we wanted to study the motion of the dynein–dynactin complex in a purified, *in vitro* system, without attachment to a bead and under conditions of minimal load, to reveal intrinsic features of force generation and motor mechano-chemistry.

RESULTS

Transgenic GFP–dynamitin mice

A transgenic mouse line was generated that expressed the dynactin subunit, dynamitin, fused to GFP. High levels of dynamitin expression result in inhibition of dynein function that leads to motor neuron degeneration, and this disruption is a graded function of the expression levels of dynamitin¹⁷. In the GFP–dynamitin line described here, expression of dynamitin is below the threshold value for disruption, and no morphological evidence of neuronal dysfunction or age-dependent neurodegeneration was observed (Fig. 1A, see Supplementary Information, Fig. S1 and data not shown).

Dynein–dynactin–GFP complexes were isolated from homogenized GFP–dynamitin mouse brains by microtubule affinity and ATP release and were purified by sucrose density gradient centrifugation. Dynein and dynactin copurified in the 20S fraction and there was no evidence of kinesin-1 or kinesin-2 in these fractions (Fig. 1B). Further purification by fast protein liquid chromatography (FPLC) was also performed¹⁸.

¹Department of Physiology and Pennsylvania Muscle Institute, University of Pennsylvania, Philadelphia, PA 19104, USA.

²Correspondence should be addressed to E.L.F.H. (e-mail: holzbaur@mail.med.upenn.edu)

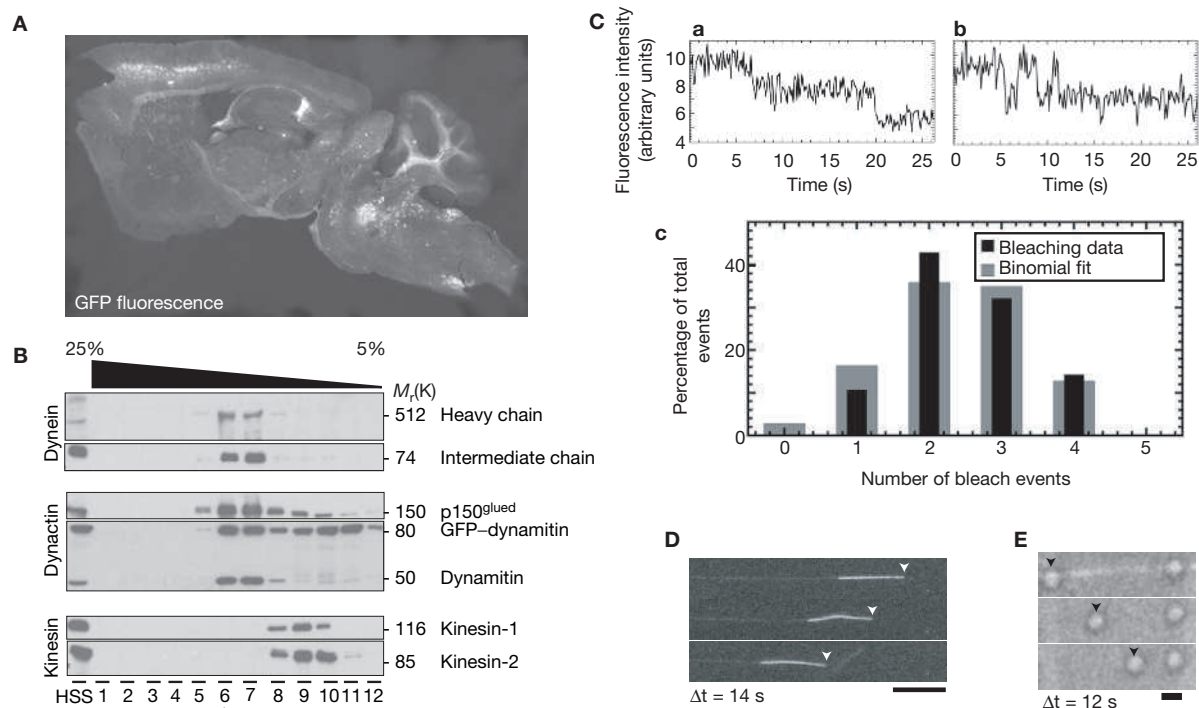


Figure 1 Purification and characterization of dynein–dynactin–GFP from GFP–dynactin mouse brains. **(A)** Epifluorescence image of a GFP–dynactin transgenic mouse brain. GFP expression is seen in the cerebellum and in patches of cell bodies in the cortex and brain stem. Expression levels are low and do not disrupt dynein–dynactin function. **(B)** Sucrose gradient fractions with dynein and dynactin subunits enriched in the same 15% sucrose fractions. Forty percent of the dynamitin in the fraction is unlabelled endogenous polypeptide and 60% is the GFP-labelled product of the transgene. Kinesins are not found in the 15% sucrose fraction with dynein–dynactin complexes. The asterisk indicates the fraction used for motility studies. For full scans of the gels and blots see Supplementary Information, Figs 2 and 4. HSS, high-speed supernatant. **(C)** Bleaching statistics for dynein–dynactin–GFP complexes

using TIRF. **(a)** A representative bleaching dataset showing two stepwise bleaching events. **(b)** A representative bleaching dataset showing that single GFPs can sometimes blink off and on. **(c)** A histogram of bleaching data for GFP complexes (black bars, $n = 181$). The average number of bleaching events is 2.2 per complex; the maximum number of bleaching events is 4. A binomial distribution with a fixed probability (P) of a GFP–dynactin incorporating into the dynactin complex is best fit when $P = 0.60$. **(D)** Microtubule-gliding assay with dynein–dynactin–GFP on the cover glass surface. The plus end of the polarity-marked microtubule is to the left. **(E)** A bead assay with dynein–dynactin–GFP coated beads shows that beads with multiple dynein motors bound move progressively towards the microtubule minus end. The scale bars indicate 10 μm in **D** and 1 μm in **E**.

These fractions displayed similar motile characteristics to the dynein–dynactin obtained directly from sucrose-density-gradient fractions (see Supplementary Information, Fig. S2).

Although previous studies have shown disruption of dynactin integrity at high dynamitin expression levels¹⁷, at the lower expression levels used here the majority of p150^{Glued} subunits cosedimented with other dynein–dynactin subunits in the approximately 20S fraction ($76 \pm 7\%$; Fig. 1B), indicating that the cocomplexes were intact. Only intact complexes were used for these studies. Western blots of purified protein indicate that approximately half of the dynamitin incorporated into the dynactin complex is GFP-labelled ($60 \pm 8\%$ GFP-labelled; $40 \pm 8\%$ unlabelled, endogenous polypeptide; Fig. 1B). The stoichiometry of GFP incorporation was further determined by stepwise bleaching using total internal reflection fluorescence (TIRF) microscopy (Fig. 1C)¹⁹. The maximum number of bleach events observed for any fluorescent particle was four, consistent with the previously determined ratio of four dynamitin subunits per dynactin complex²⁰. The average number of bleaches was 2.2. Fitting the histogram of bleaching events to a binomial probability distribution revealed that the percentage of GFP–dynactin incorporation was 60% (Fig. 1C, grey bars). This single molecule bleaching measurement is in agreement with the western blot analysis. The association of dynein with dynactin was assessed by quantitative

immunoprecipitation of the complex using an anti-dynactin antibody. The stoichiometry of binding was 0.6 dynein intermediate chains to four dynamitin subunits, indicating that three in ten GFP-labelled dynactin complexes were associated with dynein.

Ensemble motor assays display unidirectional motion

Stable dynein–dynactin complexes purified from GFP–dynactin transgenic mouse brains displayed motile properties that were identical to protein complexes purified from non-transgenic littermates in ensemble assays. In filament-gliding assays, with multiple motors moving a single microtubule, dynein from GFP–dynactin mice translocated microtubules at $650 \pm 150 \text{ nm s}^{-1}$, and dynein from wild-type mice translocated microtubules at $560 \pm 270 \text{ nm s}^{-1}$, similar to the rates observed for purified bovine brain dynein¹. Polarity-marked microtubules translocated with their plus ends forward (Fig. 1D), and beads with dynein–dynactin complexes bound were transported exclusively towards the microtubule minus end (Fig. 1E).

Single molecule assays reveal bidirectional motion

In contrast with ensemble assays, single dynein–dynactin–GFP complexes displayed novel motion when observed using total internal reflection fluorescence (TIRF) microscopy, which allows visualization of

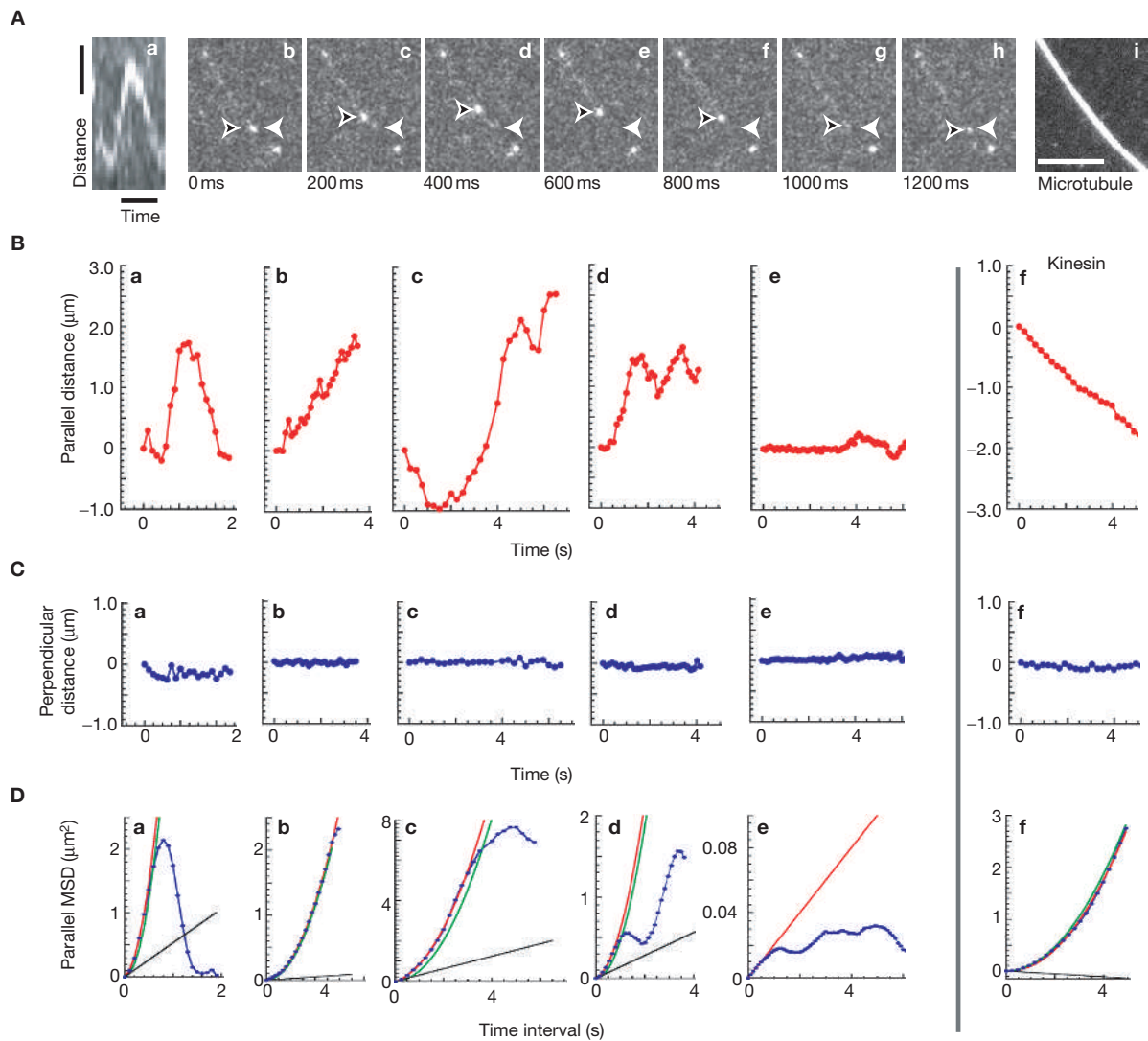


Figure 2 Example traces of motion exhibited by dynein-dynactin-GFP as visualized by TIRF. **(A)** Time series and analysis of dynein-dynactin-GFP motion for a dataset at 10 mM ATP. **(a)** A kymograph from time-series data shows clear reversal of direction with long processive motion in each direction. The vertical scale bar represents 1 μm and the horizontal scale bars represents 1 s. **(b-h)** A time series of dynein-dynactin-GFP moving along the microtubule. The white arrowhead indicates the starting position of the complex. The black arrowhead indicates the location at each time point. **(i)** An epifluorescence image of a rhodamine-labelled microtubule. The scale bar represents 4 μm . **(B)** **(a-e)** Single molecules traces of dynein-dynactin-

GFP movements parallel to the microtubule. **(f)** Example trace of kinesin-GFP motility parallel to the microtubule, for comparison. **(C)** **(a-e)** Single molecules traces of dynein-dynactin-GFP movements perpendicular to the microtubule. **(f)** Example trace of kinesin-GFP motility perpendicular to the microtubule, for comparison. **(D)** **(a-e)** The MSD of single molecule traces of dynein-dynactin-GFP. **(f)** Example MSD for kinesin-GFP trace. The blue circles are the calculated MSD from the parallel traces in **(B)**. The red curve is the fit equation $p(t) = v^2 t^2 + 2Dt$. The green curve is the deterministic contribution to the fit ($v^2 t^2$) only. The black line is the random contribution to the fit ($2Dt$) only. See Methods for details.

single motor complexes. Epifluorescence was used to identify a polarity-marked microtubule by rhodamine fluorescence (Fig. 2A, i). To observe individual GFP-labelled complexes, samples were excited with 488 nm laser light and sequences were recorded in the GFP fluorescence channel at 10–30 frames per second. A time series from a data set taken at 10 frames per second shows a single fluorescent complex moving along the microtubule (Fig. 2A, b–h and see Supplementary Information, Movie 1). The image sequences were analysed in two manners: first, successive GFP images were placed along the microtubule in sequential order to create kymograph images that depict motion (Fig. 2A, a); second, a two-dimensional Gaussian fitting routine was used to track the position of individual spots over time (Fig. 2B, C). Several distinct types of motion were observed for individual dynein-dynactin-GFP

complexes, including processive segments (Fig. 2B, a–d), as well as bidirectional (Fig. 2B, a, c, d), and diffusive (Fig. 2B, e) motion. A processive run is defined here as motion in the same direction for >3 successive sequence frames travelling >300 nm. Dynein-dynactin complexes often showed bidirectional excursions. Some bidirectional excursions seemed random, suggesting diffusive motion (Fig. 2B, b, d). Other bidirectional motion was processive in both directions, exhibiting runs that sometimes extended $\geq 1 \mu\text{m}$ towards both the minus and plus ends (Fig. 2B, a, c). In comparison, GFP-kinesin tracked by the same methods was smoothly processive and unidirectional (Fig. 2B, f).

Analysis of single molecule data revealed that 30% of processive runs were directed toward the plus ends of polarity-marked microtubules (Fig. 3a). Although previous studies raised the possibility of

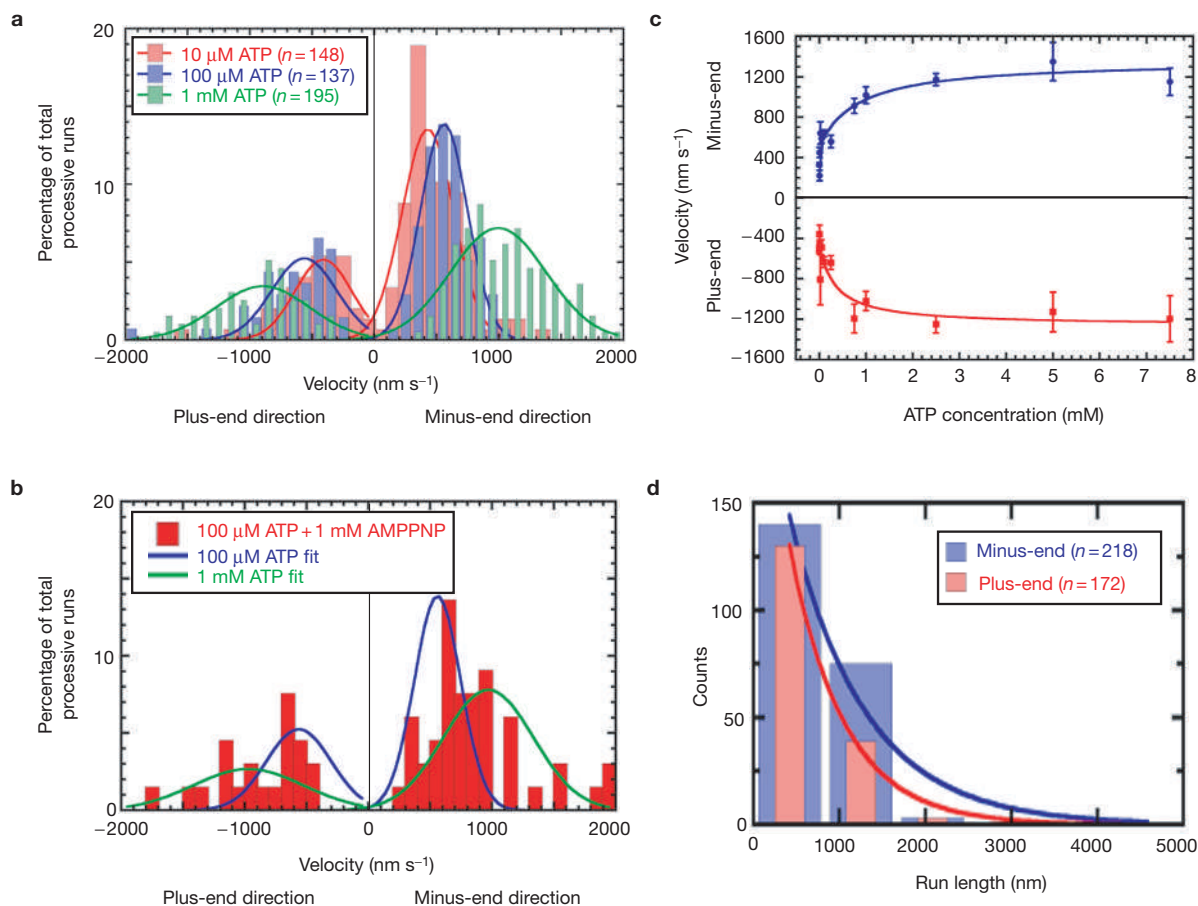


Figure 3 Histograms of velocities of individual dynein–dynactin–GFP complexes exhibiting processive runs. **(a)** Histograms of the velocities of processive runs (>300 nm) are plotted for $10\ \mu\text{M}$ ATP (red bars, $n = 148$), $100\ \mu\text{M}$ ATP (blue bars, $n = 137$) and $1\ \text{mM}$ ATP (green bars, $n = 195$). Histograms were normalized by dividing by the total number of events so that the area under each curve is equal to 100%. At all three ATP concentrations, 30% of motions are plus-end directed. Gaussian fits to the histograms (solid lines; $10\ \mu\text{M}$, red; $100\ \mu\text{M}$, blue; $1\ \text{mM}$, green) show that the distributions are similar in the minus-end and plus-end directions. The mean velocity increases in both directions as ATP concentration increases. **(b)** Histogram of velocities observed in the presence of $1\ \text{mM}$ AMPPNP plus $100\ \mu\text{M}$ ATP (red

bars) compared with velocities observed at either $100\ \mu\text{M}$ ATP (blue fit line) or $1\ \text{mM}$ ATP (green fit line) only. AMPPNP did not inhibit bidirectional motion of dynein–dynactin–GFP and caused much higher velocities than expected with $100\ \mu\text{M}$ ATP. **(c)** For individual dynein–dynactin–GFP complexes that reversed direction on the same microtubule, the velocities in either direction were similar over all ATP concentrations (minus end, blue circles and line; plus end, red squares and line). The error bars represent the s.e.m. for more than five separate trials. **(d)** For individual dynein–dynactin–GFP complexes that reversed direction on the same microtubule, the run lengths are slightly longer in the minus-end direction (blue bars and blue line exponential fit, $n = 218$) than the plus-end direction (red bars and red line exponential fit, $n = 172$).

dynein–dynactin bidirectionality^{13,21–23}, single-molecule assays provide unambiguous evidence of the bidirectional nature of the dynein–dynactin complex. Histograms of the velocities show that minus-end and plus-end directed runs display similar dependence of the average velocities on the ATP concentration (Fig. 3a). Many individual complexes (30% of $n = 510$) displayed bidirectional motion, where a single complex switched from a processive minus-end run to a processive plus-end run on the same microtubule (Fig. 2B, a, c, d).

For complexes that reversed direction, the average velocities in either direction were almost identical over a large range of ATP concentrations (Fig. 3c). Histograms of run lengths for complexes that reversed direction showed minus-end directed (880 ± 180 nm) and plus-end directed (630 ± 50 nm) runs (Fig. 3d). The minus-end run lengths are slightly shorter than those previously reported using bead assays^{12,24}, which is consistent with the slower diffusion of beads away from the microtubule in comparison with undocked proteins. The average plus-end run lengths are significantly longer than those previously reported for dynein alone bound to beads²². The characteristics of the motion, velocity and

run length were similar in both directions. However, there was an overall bias towards minus-end motion in both frequency and run length, consistent with the results of ensemble assays.

To analyse the processive nature of the bidirectional motility, the mean squared displacement (MSD) of the single particle traces was plotted versus the time interval, which allowed a quantitative measure of deterministic and random contributions to movement (see Methods for details of MSD calculation and fitting)^{13,25}. Of the 40 tracked particles, 60% included a significant deterministic component of the MSD over the time intervals of 2–5 s (Fig. 2D, a–d). This feature implies temporal correlation of velocities due to multiple successive steps in the same direction. Particles that reversed direction display a MSD that switches from increasing to decreasing due to the reversal of processive motion (Fig. 2D, a, c, d).

All position traces for motion parallel to the microtubule axis included a significant diffusive component to the MSD resulting in an average diffusion coefficient of $5.8 \pm 0.2 \times 10^{-10}\ \text{cm}^2\ \text{s}^{-1}$ (s.e.m., $n = 40$). In a previous study using $200\ \text{nm}$ dynein-coated beads, the beads exhibited

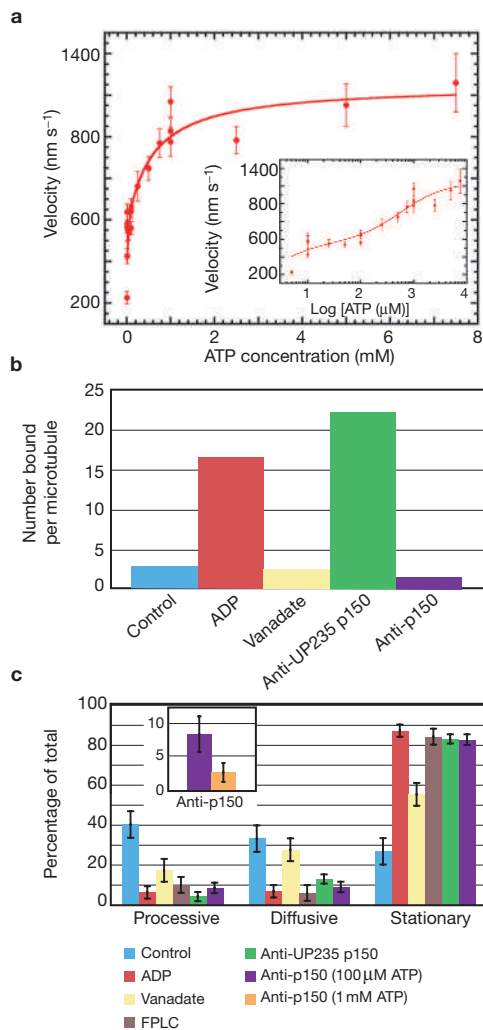


Figure 4 ATP dependence of average velocity and the effects of dynein inhibitors. **(a)** The average velocity of processive runs (>300 nm) of dynein–dynactin–GFP complexes depends on ATP concentration with two sets of Michaelis-Menton constants. The inset showing the velocity as a function of the log[ATP concentration] emphasizes the data and fit at low ATP concentrations. The error bars represent the s.e.m. for >15 separate trials. **(b)** The number of GFP-complexes bound per microtubule for five randomly selected microtubules when only 100 μM ATP is present (control, blue bars), no ATP is present (20 μM ADP, red bars), vanadate is present (100 μM ATP + 100 μM vanadate, yellow bars), UP235 polyclonal p150^{GluEd} antibody is present (100 μM ATP, green bars) and mouse monoclonal p150^{GluEd} antibody is present (100 μM ATP, purple bars). **(c)** Percent of dynein–dynactin–GFP molecules that exhibit processive runs (>300 nm), motion that had no processive segments (termed ‘diffusive’) and non-moving stationary behaviour, when 100 μM ATP is present (control, blue bars), no ATP is present (20 μM ADP, red bars), vanadate is present (100 μM ATP + 100 μM vanadate, yellow bars), FPLC-purified dynactin–GFP complexes (100 μM ATP, brown bars), UP235 polyclonal p150^{GluEd} antibody is present (100 μM ATP, green bars) and mouse monoclonal p150^{GluEd} antibody is present (100 μM ATP, purple bars). The error bars represent the s.e.m. for five separate trials. There is significant depression of directed and diffusive motion without ATP, with vanadate or with antibodies (Student’s *t*-test, $P < 0.01$; number of microtubules analysed >8). The inset indicates that, in the presence of mouse monoclonal antibody to p150^{GluEd}, fewer complexes exhibit processive motion at 1 mM ATP (orange bar) than at 100 μM ATP (purple bar; Student’s *t*-test, $P = 0.06$, $n = 20$) suggesting that dynactin helps to tether dynein to microtubules.

one-dimensional diffusion along microtubules, with a diffusion constant of $2.2 \times 10^{-10} \text{ cm}^2 \text{ s}^{-1}$ (ref. 13). As the dynein–dynactin complex is several times smaller than 200 nm beads, the diffusion coefficients of the two studies are consistent.

The perpendicular-position traces displayed smaller displacements than the parallel direction, as is expected for molecules moving along microtubules (Fig. 2C). The uncertainty and noise in the position trace was determined by tracking a stationary complex bound to the cover glass for each movie (s.d. = 11 nm). On average, the perpendicular displacements above the noise in tracking are approximately 25 nm (the approximate diameter of the microtubule), suggesting that a dynein–dynactin complex may wander across the microtubule, switching protofilaments as it steps, as previously proposed¹³.

Dynein–dynactin motors display unique mechano-chemistry

TIRF assays were performed over a wide range of ATP concentrations (5 μM–7.5 mM MgATP) and the average velocity of processive runs (>300 nm) toward the microtubule minus-end clearly increased with ATP concentration (Fig. 4a). The data could not be fit with a single set of Michaelis-Menton constants (see Supplementary Information, Fig. S3), but instead required a model with at least two sets of ATP-dependent parameters, consistent with multiple ATP sites within each motor domain. The average velocities were within the range of velocities previously reported for dynein studied by filament-gliding and bead assays^{12,24,26}, and are consistent with a report that cytoplasmic dynein displayed two sets of kinetic constants in filament-gliding assays at various ATP concentrations²⁶. The structure of the ring-shaped dynein motor domain, with multiple adjacent nucleotide binding sites, suggests that a conformational interaction or ‘communication’ may propagate around the ring as in other AAA domain proteins^{27,28}. Biochemical evidence shows that ATP binding, and possibly hydrolysis at the regulatory site, AAA3, enhances ATPase activity at AAA1 indicating communication between these modules^{5,15}. This interaction could modulate the velocity and force of the motor when nucleotide is bound and/or cleaved at the regulatory site.

Dynein–dynactin complexes must bind and hydrolyse ATP for processive bidirectional motility

Processive motion of single dynein–dynactin–GFP complexes required ATP binding and hydrolysis. In the absence of ATP (20 μM ADP), the number of complexes bound per microtubule increased approximately sixfold compared with experiments where ATP was present (Fig. 4b), which is consistent with tight microtubule binding of ADP–dynein complexes²⁹. The percentage of complexes exhibiting processive runs (>300 nm) was reduced from 40% to 6%, and the percentage of stationary complexes increased from 26% to 87% (Fig. 4c, red bars). The addition of 100 μM vanadate, a transition state analogue that traps dynein in an ADP–V_i state, significantly reduced binding to microtubules (Fig. 4b). The percentage of complexes exhibiting processive runs was reduced from 40% to 14%, and the percentage of stationary complexes increased from 26% to 55% (Fig. 4c, yellow bars). Taken together, these results indicate that ATP binding and hydrolysis are required for processive motion. Interestingly, the percentage of complexes displaying diffusive motion is almost the same with (28%) or without vanadate (33%; Fig. 4c). The diffusive motion and stationary binding observed in the presence of vanadate may be due to direct, ATP-insensitive, dynactin binding to the

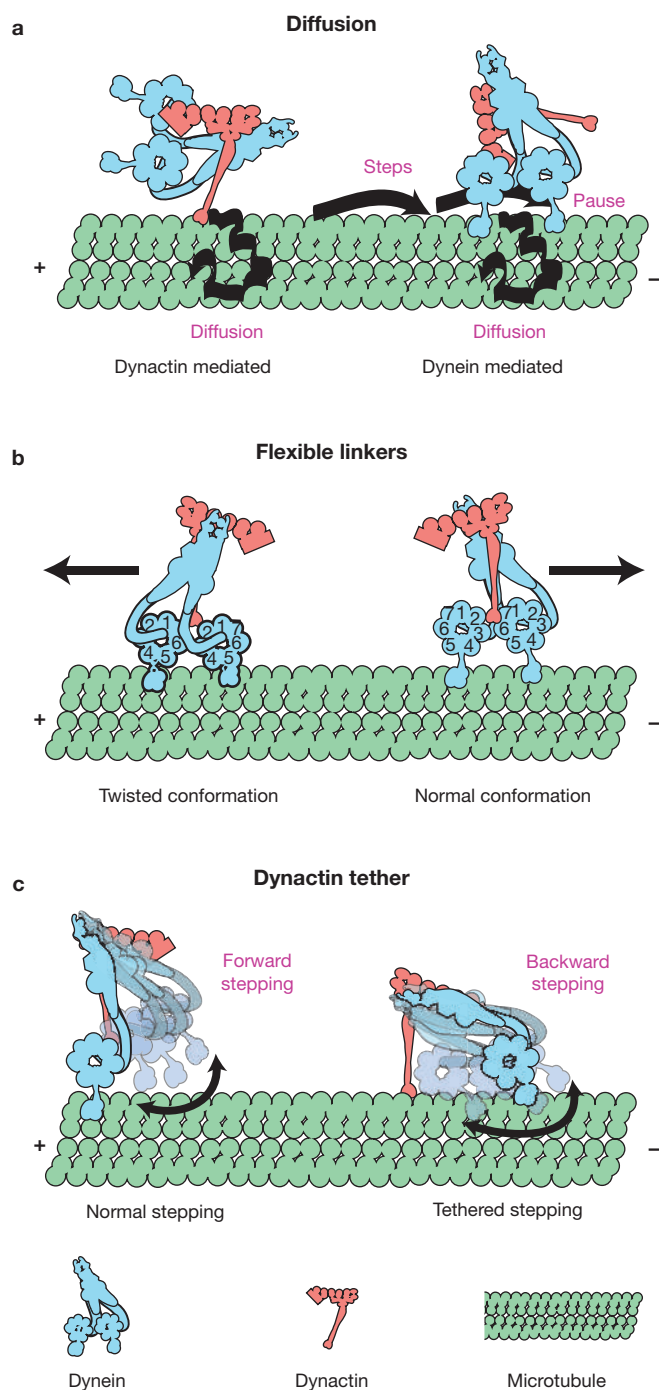


Figure 5 Possible models for the bidirectional motility observed for dynein–dynactin. (a) Some of the bidirectional motions may be due to random, diffusive motions that are either mediated by dynactin attachment through its basic microtubule-binding domain, with or without dynein, or dynein binding loosely and diffusing during a pause after taking successive forward steps. (b) The flexible structure of dynein may allow rotation of the AAA ring such that the motor strokes in the opposite direction. (c) Dynein may take a variety of step sizes, forward or backward, as dictated by the microtubule-lattice spacing. If dynactin tethers the dynein to the microtubule so as to bias the diffusive search for the next binding site, the dynein could take multiple steps in the plus-end direction.

microtubule. Indeed, a recent study showed that recombinant fragments of the microtubule-binding p150^{Glued} subunit of dynactin could cause bead ‘skating’ along the microtubule³⁰. In agreement with our observations, 28% of beads bound with recombinant full-length p150^{Glued}, or various fragments of p150^{Glued}, showed diffusive motion³⁰.

Dynein is required for processive movement of GFP–dynactin complexes

Processive motion of GFP-labelled complexes required dynein. Dynein and dynactin–GFP were separated by anion exchange FPLC¹⁸. Although some residual dynein remained, as previously reported¹⁸, the removal of most dynein motors reduced the percentage of processive complexes to 10% and increased the percentage of stationary complexes to 84% (Fig. 4c, brown bars). The complexes that displayed processive motion moved bidirectionally, with velocities identical to the complexes purified by sucrose gradient alone at the same ATP concentrations (see Supplementary Information, Fig. S2). Only 5% of the dynactin–GFP complexes displayed diffusion-like motion that could be attributed to dynactin, which is much less than that reported for recombinant dynactin bound to beads³⁰. This suggests that, for the most part, our preparation of GFP–dynactin statically locks on to the microtubule through the CAP–Gly domain. Interestingly, we found that when ADP–V_i was added to dynein–dynactin–GFP to inactivate the dynein motility, diffusive motions were observed, with similar statistics to those reported for the basic domain of dynactin bound to beads³⁰. This suggests that dynein binding to dynactin may have an allosteric effect that inactivates the statically binding CAP–Gly domain of p150^{Glued} and simultaneously activates the basic domain, which is responsible for skating.

A polyclonal antibody against p150^{Glued}, UP235, is known to block dynein–dynactin association and inhibit dynein-mediated vesicular transport in extruded axoplasm⁹. When UP235 was incubated with dynein–dynactin–GFP, the number of complexes bound per microtubule increased approximately eightfold compared with that observed without antibody (Fig. 4b). The percentage of complexes exhibiting processive runs decreased from 40% to 4%, and the percentage of stationary complexes increased from 26% to 83% compared with experiments without antibody (Fig. 4c, green bars). This condition is similar to the rigor-like state observed when this antibody was added to squid axoplasm⁹. Together, these results indicate that dynein is required for processive motion of the dynactin–GFP complexes.

Dynactin tethers the dynein–dynactin complex to microtubules

A monoclonal antibody against p150^{Glued} binds to the CAP–Gly microtubule-binding motif of the p150^{Glued} subunit. This antibody reduced the number of complexes binding to the microtubules by 47% (Fig. 4b). The percentage of complexes exhibiting processive runs decreased from 40% to 8%, and the percentage of stationary complexes increased from 26% to 83% (Fig. 4c, purple bars). Although the antibody did not affect the velocity of the processive complexes, the inhibition of processive motility by this monoclonal antibody was stronger at higher ATP concentrations (1 mM versus 100 μ M; Fig. 4c, inset). It is predicted that dynein is a motor that spends a small proportion of its ATPase cycle bound to microtubules (low-duty ratio), therefore, increasing ATP concentration will increase the chance that both heads of the molecule will simultaneously detach from the microtubules²⁹. The strong dissociation effect of the monoclonal antibody at high ATP concentration suggests

that dynactin tethers the complex to the microtubule, thereby increasing processivity^{12,31}. Thus, dynactin acts as a non-obligate tether for single dynein motors that enhances the association of dynein with the microtubule at high ATP concentrations, but is not required for the processive motility of dynein.

AMPPNP does not inhibit bidirectional motion

Control experiments were performed to test whether the processive plus-end runs observed for GFP-labelled complexes may be due to copurification of kinesin, as previous work has shown that dynein and kinesin-2 compete for the same site on dynactin³². Western blots of the purified motor complex that were probed for kinesin-1 and kinesin-2 showed that neither of these plus-end-directed motors were present in the dynein–dynactin fractions used in motility assays (Fig. 1B). To test for residual kinesin activity, 1 mM AMPPNP, a non-hydrolysable analogue of ATP, was added with 100 μ M ATP to the dynein–dynactin–GFP TIRF motility assay. Under these conditions, any kinesin present should tightly bind to microtubules, but dynein should be motile^{33–35}. AMPPNP did not inhibit motility of dynein–dynactin–GFP complexes in either the plus-end or minus-end directions. Surprisingly, the addition of AMPPNP in the presence of 100 μ M ATP resulted in increased velocity of motility, almost to that observed at 1 mM ATP (Fig. 3b). We hypothesize that AMPPNP may bind to one of the secondary AAA modules of dynein, possibly the AAA3 regulatory site, and act as an allosteric activator that leads to an increase in velocity due to conformational changes around the motor domain ring.

DISCUSSION

This study provides the first evidence that a native microtubule-based motor protein can display processive motion in both directions along the microtubule. Previous studies using single dynein molecules bound to small beads have shown that dynein can display a diffusive mode of bidirectional motion along the microtubule in the absence of dynactin^{13,22}. In contrast with the robust, long-range, plus-end motion observed in our study (30% of all motion over 300 nm), a previous study reported that a small fraction of the plus-end motion displayed run lengths greater than 300 nm (13% of plus-end motion; 2% of total directed segments)²². One significant difference between the two studies is the presence of dynactin in our single molecule fluorescence study. A possible explanation for these results is that dynactin increases the processivity of motion in the plus-end, as well as the minus-end direction, as dynactin can bind microtubules loosely and diffuse along the surface in a bidirectional manner³⁰.

Several models would explain the robust bidirectional motion observed in this study. One possibility is that plus-end runs are diffusive, mediated either by the direct binding of dynactin to the microtubule or by a diffusive mode of dynein, as previously postulated¹³ (Fig. 5a). However, this model does not explain the processive runs (>300 nm) in the plus-end direction, nor the ATP dependence of their velocity. A second possibility is that plus-end runs are composed of steps in the plus-end direction that are driven by dynein twisted around the stalk so that the power stroke is in the opposite direction (Fig. 5b). This hypothesis is supported by the similar ATP dependence of the velocity in both directions (Fig. 3c) and the flexible nature of the dynein heavy chain². A third possibility is that plus-end runs are backward steps that result from dynactin tethering the dynein with a plus-end directed bias (Fig. 5c).

Minus-end stepping of dynein is known to vary in size, presumably due to the flexibility of dynein¹⁶, and this same flexibility may lead to several backward steps in a row.

In current models of microtubule-based transport in the cell, kinesin is always plus-end directed and dynein is always considered to be minus-end directed. It is thus postulated that the bidirectional motility of vesicular and macromolecular cargoes observed *in vivo* is due to reciprocal regulation of dynein and kinesin motors. However, multiple studies have shown that reducing dynein function with inhibitory antibodies or small interfering RNA molecules causes a block in both plus- and minus-end-directed transport in cells^{9,36,37}. In addition, endocytosed quantum dots, transported in cells by motor proteins, were observed to take large 16-nm steps in the plus-end direction that were similar to those observed in the minus-end direction; these steps are consistent with dynein, rather than kinesin, mechano-chemistry³⁸. Through direct observations of single molecules of purified dynein–dynactin complexes, we see bidirectional motion *in vitro*; thus it is possible that dynein may contribute to plus-end, as well as to minus-end, directed transport in the cell.

The ability to switch directions may be affected by load, and therefore, the bidirectional motility described here may be most relevant to the dynein-mediated transport of smaller macromolecular cargoes, such as RNA or individual proteins in the cell. Using an optical trapping technique, it has been shown that vesicular cargoes are transported by multiple motors *in vivo*³⁹. The presence of multiple dynein motors will enhance processivity toward the minus-end, as observed in ensemble bead assays. However, the ability to make backward excursions, as described here, combined with the flexibility of the dynein–dynactin complex, may be an advantage when navigating through the crowded cellular environment. □

METHODS

Generation and maintenance of transgenic mice. Full-length human cDNA for *dynamitin* was modified to include an enhanced green fluorescent protein (EGFP) label fused to the C-terminus, and subcloned into the *Xho*I site of the Thy1.2 mouse expression cassette, a gift from P. Caroni (Friedrich Miescher Institute, Basel, Switzerland). The DNA was submitted to the Transgenic and Chimeric Mouse Facility at the University of Pennsylvania for injection into B6SJL fertilized mouse eggs. Subsequent generations of the positive GFP–*dynamitin* mice were maintained in the B6SJL hybrid background. Mice hemizygous for the transgene were identified by PCR using the primers GGATCTCAAGCCCTCAAG and CTTGGACCTCATGCAGTAGG. The IACUC committee at the University of Pennsylvania approved all animal protocols. Brains were harvested from approximately 4-month-old hemizygous mice immediately after euthanasia by an overdose of isoflurane followed by decapitation.

Protein purification. Cytoplasmic dynein associated with dynactin was purified from mouse brain by microtubule-affinity ATP extraction and sucrose gradient centrifugation as previously described⁴⁰. The protein was flash frozen with 10 μ M ATP and 25% sucrose in liquid nitrogen and stored at -80 °C. The integrity of the complex was assayed by SDS–PAGE and western blot probing for dynein heavy chain (antibody Am#8, a gift from R. Vallee; Columbia University, NY), dynein intermediate chain (MAB 1618, Chemicon, Temecula, CA), p150^{Glued} (monoclonal, BD Transduction Laboratories, San Jose, CA), dynamitin (monoclonal, BD Transduction Laboratories), kinesin heavy chain (MAB1614, Chemicon) and kinesin-2 (K2.4, a gift from V. Gelfand, Northwestern University, Chicago, IL). FPLC purification was performed on a Mono Q HR 10/10 anion exchange column (Pharmacia Biotech, Piscataway, NJ) using a previously described elution sequence¹⁸.

Stoichiometry determination of dynein–dynactin complex. There are four dynamitin subunits per dynein–dynactin complex; therefore, up to four GFP-labelled

dynamitins were expected to incorporate into the dynactin complex. Western blot analysis showed that 60% of the total dynamitin in the sucrose gradient fraction used for experiments was GFP-labelled. Individual dynein–dynactin–GFP complexes were observed to photobleach in a stepwise manner (Fig. 1C), as previously reported for GFP–kinesin¹⁹.

If the GFP–dynamitin distributes randomly into the available binding sites, then the number, n , of bleach events due to GFP would be described by the binomial distribution:

$$P(n, N) = \frac{N!}{n!(N-n)!} p^n (1-p)^{N-n}$$

where N is the maximum number of sites ($N = 4$, $0 \leq n \leq N$), p is the probability that any individual site is occupied by a GFP–dynamitin, and the exclamation point denotes the factorial function. The bleaching distribution is best fit by a binomial distribution with $N = 4$ and $p = 0.60$ (Fig. 1D, grey bars). The agreement between these values and the average incorporation in the western blot assay indicates that there are a maximum of four sites per complex and the GFP label neither hindered nor facilitated incorporation of multiple dynamitins into the dynactin complex during assembly.

Quantitative immunoprecipitation was performed to determine the stoichiometry of dynein to dynactin in our preparations. Immunoprecipitation was performed using a monoclonal antibody against the CAP–Gly domain of the p150^{Glued} dynactin subunit. The quantity of dynamitin or dynein intermediate chain peptide in the immunoprecipitate was compared to a standard dilution series of recombinant subunits on the same western blot.

In vitro motility assay. Assays were performed in a flow chamber (volume approximately 8 μ l) made from two-glass cover slips attached with double-sided adhesive tape. Taxol stabilized, polarity marked, microtubules were made by growing dim segments (1:50 rhodamine labelling) from bright seeds (1:5 rhodamine labelling). The segment that grew longer was denoted as the plus end. Polarity was further verified using GFP–kinesin. Microtubules were allowed to flow into the chamber and to bind non-specifically to the cover glass and then the chamber was blocked with 5 mg ml⁻¹ casein in assay buffer (10 mM PIPES, 35 mM potassium acetate, 5 mM MgSO₄, 5 mM EDTA and 10 mM Taxol). ATP was added to motility buffer as noted in the text. Nucleotide concentrations were checked post-experiment by running the same samples on an ion-exchange high-pressure liquid chromatography column to separate ATP from ADP and comparing to a standard sample of known ATP and ADP concentrations. Single dynein–dynactin–GFP complexes were visualized at 25 °C by TIRF excited by a 488-nm Argon-ion laser on an inverted microscope (Olympus IX70), and recorded by an Andor back-thinned DX677 video camera at various frame rates (10–33 frames per second). Kymographs were made using the ‘Multiple Kymograph’ plug-in for ImageJ submitted to <http://rsb.info.nih.gov/ij/> by J. Rietdorf and A. Seitz (European Molecular Biology Laboratory, Heidelberg, Germany). For studies with dynactin antibodies, affinity-purified polyclonal p150^{Glued} antibody (UP235) was incubated at a 0.2 mg ml⁻¹ or monoclonal p150^{Glued} antibody (BD Transduction Laboratories) was incubated at 0.025 mg ml⁻¹ with dynein–dynactin–GFP and 100 μ M ATP for 20 min.

Particle tracking analysis. Two dimensional Gaussian fitting and particle tracking were performed on dynein–dynactin–GFP complexes that were bright and well separated from nearby fluorophores using a plug-in specifically written in our laboratory for ImageJ. Displacements parallel and perpendicular to the microtubules were calculated as projections onto unit vectors tangent and orthogonal to the microtubule²⁵. Motions parallel to the microtubule were used to compute the MSD for each position trace. For a given time interval, the MSD is the average of the squares of the difference in the position¹³. Plots of the MSD against the time interval were fit over the first several time intervals to the equation: $\rho(t) = v^2 t^2 + 2Dt$, where v is the velocity of the correlated, processive contribution to the motion, and D is the random, diffusive contribution (Fig. 2D)^{13,25}. See Supplementary Information, Methods for a full description of the MSD analysis.

Inspection for bundled microtubules. Experiments were performed to determine if adjacent, oppositely directed, microtubules may provide bidirectional tracks. Pairs and bundles of fluorescently labelled microtubules were easy to distinguish from single microtubules as the fluorescence intensity of two microtubules next to each other was noticeably increased. Processive motion of

GFP-labelled kinesin motors (the plasmid for which was a gift from R. Vale, University of California, San Francisco, CA) was always in one direction along the same polarity-marked microtubules. This observation suggests that the corresponding microtubules provided single unidirectional tracks. Thus, the bidirectional motion of the dynein–dynactin–GFP complexes was not due to the complexes switching tracks between two nearby microtubules.

Statistical methods. For all measurements, the error bars represent the s.e.m. Statistical significance was determined by comparing data sets with different numbers of trials using the Student's t -test on unpaired data with unequal variance. Probability values and number of trials are given in the text or figure captions where appropriate.

Note: Supplementary Information is available on the Nature Cell Biology website.

ACKNOWLEDGMENTS

This work was supported by a National Institutes of Health (NIH) project program grant (P01-AR-051174) to the Pennsylvania Muscle Institute, by an ALS Association grant to E.L.F.H., and J.L.R. is supported by an NIH NRSA grant (1F32GM075754-01). The authors also thank A. Loh, R. Kudaravalli, H. Pham, W. Zhou and M. Tokito.

COMPETING FINANCIAL INTERESTS

The authors declare that they have no competing financial interests.

Published online at <http://www.nature.com/naturecellbiology/>

Reprints and permissions information is available online at <http://npg.nature.com/reprintsandpermissions/>

- Paschal, B. M. & Vallee, R. B. Retrograde transport by the microtubule-associated protein MAP 1C. *Nature* **330**, 181–183 (1987).
- Burgess, S. A., Walker, M. L., Sakakibara, H., Knight, P. J. & Oiwa, K. Dynein structure and power stroke. *Nature* **421**, 715–718 (2003).
- Ogawa, K. Four ATP-binding sites in the midregion of the β heavy chain of dynein. *Nature* **352**, 643–645 (1991).
- Gibbons, I. R. *et al.* Photosensitized cleavage of dynein heavy chains: Cleavage at the ‘V1 site’ by irradiation at 365 nm in the presence of ATP and vanadate. *J. Biol. Chem.* **262**, 2780–2786 (1987).
- Kon, T., Nishiura, M., Ohkura, R., Toyoshima, Y. Y. & Sutoh, K. Distinct functions of nucleotide-binding/hydrolysis sites in the four AAA modules of cytoplasmic dynein. *Biochemistry* **43**, 11266–11274 (2004).
- Takahashi, Y., Edamatsu, M. & Toyoshima, Y. Y. Multiple ATP-hydrolyzing sites that potentially function in cytoplasmic dynein. *Proc. Natl Acad. Sci. USA* **101**, 12865–12869 (2004).
- Schroer, T. A. Dynactin. *Annu. Rev. Cell Dev. Biol.* **20**, 759–779 (2004).
- Schroer, T. A. & Sheetz, M. P. Two activators of microtubule-based vesicle transport. *J. Cell Biol.* **115**, 1309–1318 (1991).
- Waterman-Storer, C. M. *et al.* The interaction between cytoplasmic dynein and dynactin is required for fast axonal transport. *Proc. Natl Acad. Sci. USA* **94**, 12180–12185 (1997).
- Levy, J. R. *et al.* A motor neuron disease-associated mutation in p150^{Glued} perturbs dynactin function and induces protein aggregation. *J. Cell Biol.* **172**, 733–745 (2006).
- Puls, I. *et al.* Mutant dynactin in motor neuron disease. *Nature Genet.* **33**, 455–456 (2003).
- King, S. J. & Schroer, T. A. Dynactin increases the processivity of the cytoplasmic dynein motor. *Nature Cell Biol.* **2**, 20–24 (2000).
- Wang, Z. & Sheetz, M. P. One-dimensional diffusion on microtubules of particles coated with cytoplasmic dynein and immunoglobulins. *Cell Struct. Funct.* **24**, 373–383 (1999).
- Ishii, Y., Nishiyama, M. & Yanagida, T. Mechano-chemical coupling of molecular motors revealed by single molecule measurements. *Curr. Protein Pept. Sci.* **5**, 81–87 (2004).
- Kon, T., Mogami, T., Ohkura, R., Nishiura, M. & Sutoh, K. ATP hydrolysis cycle-dependent tail motions in cytoplasmic dynein. *Nature Struct. Mol. Biol.* **12**, 513–519 (2005).
- Mallik, R., Carter, B. C., Lex, S. A., King, S. J. & Gross, S. P. Cytoplasmic dynein functions as a gear in response to load. *Nature* **427**, 649–652 (2004).
- LaMonte, B. H. *et al.* Disruption of dynein/dynactin inhibits axonal transport in motor neurons causing late-onset progressive degeneration. *Neuron* **34**, 715–727 (2002).
- Bingham, J. B., King, S. J. & Schroer, T. A. Purification of dynactin and dynein from brain tissue. *Methods Enzymol.* **298**, 171–184 (1998).
- Vale, R. D. *et al.* Direct observation of single kinesin molecules moving along microtubules. *Nature* **380**, 451–453 (1996).
- Schafer, D. A., Gill, S. R., Cooper, J. A., Heuser, J. E. & Schroer, T. A. Ultrastructural analysis of the dynactin complex: An actin-related protein is a component of a filament that resembles F-actin. *J. Cell Biol.* **126**, 403–412 (1994).
- Euteneuer, U., Koonce, M. P., Pfister, K. K. & Schliwa, M. An ATPase with properties expected for the organelle motor of the giant amoeba, *Reticulomyxa*. *Nature* **332**, 176–178 (1988).

22. Mallik, R., Petrov, D., Lex, S. A., King, S. J. & Gross, S. P. Building complexity: An *in vitro* study of cytoplasmic dynein with *in vivo* implications. *Curr. Biol.* **15**, 2075–2085 (2005).
23. Wang, Z., Khan, S. & Sheetz, M. P. Single cytoplasmic dynein molecule movements: Characterization and comparison with kinesin. *Biophys. J.* **69**, 2011–2023 (1995).
24. Wang, Z. & Sheetz, M. P. The C-terminus of tubulin increases cytoplasmic dynein and kinesin processivity. *Biophys. J.* **78**, 1955–1964 (2000).
25. Okada, Y. & Hirokawa, N. A processive single-headed motor: kinesin superfamily protein KIF1A. *Science* **283**, 1152–1157 (1999).
26. Shimizu, T., Toyoshima, Y. Y., Edamatsu, M. & Vale, R. D. Comparison of the motile and enzymatic properties of two microtubule minus-end-directed motors, ncd and cytoplasmic dynein. *Biochemistry* **34**, 1575–1582 (1995).
27. Hersch, G. L., Burton, R. E., Bolon, D. N., Baker, T. A. & Sauer, R. T. Asymmetric interactions of ATP with the AAA+ ClpX₆ unfoldase: Allosteric control of a protein machine. *Cell* **121**, 1017–1027 (2005).
28. Mancini, E. J. *et al.* Atomic snapshots of an RNA packaging motor reveal conformational changes linking ATP hydrolysis to RNA translocation. *Cell* **118**, 743–755 (2004).
29. Holzbaur, E. L. & Johnson, K. A. Microtubules accelerate ADP release by dynein. *Biochemistry* **28**, 7010–7016 (1989).
30. Culver-Hanlon, T. L., Lex, S. A., Stephens, A. D., Quintyne, N. J. & King, S. J. A microtubule-binding domain in dynactin increases dynein processivity by skating along microtubules. *Nature Cell Biol.* **8**, 264–270 (2006).
31. Waterman-Storer, C. M., Karki, S. & Holzbaur, E. L. F. The p150^{Glued} component of the dynactin complex binds to both microtubules and the actin-related protein centractin (Arp-1). *Proc. Natl Acad. Sci. USA* **92**, 1634–1638 (1995).
32. Deacon, S. W. *et al.* Dynactin is required for bidirectional organelle transport. *J. Cell Biol.* **160**, 297–301 (2003).
33. Lasek, R. J. & Brady, S. T. Attachment of transported vesicles to microtubules in axoplasm is facilitated by AMP-PNP. *Nature* **316**, 645–647 (1985).
34. Murray, J. W., Bananis, E. & Wolkoff, A. W. Reconstitution of ATP-dependent movement of endocytic vesicles along microtubules *in vitro*: An oscillatory bidirectional process. *Mol. Biol. Cell* **11**, 419–433 (2000).
35. Vale, R. D., Reese, T. S. & Sheetz, M. P. Identification of a novel force-generating protein, kinesin, involved in microtubule-based motility. *Cell* **42**, 39–50 (1985).
36. He, Y. *et al.* Role of cytoplasmic dynein in the axonal transport of microtubules and neurofilaments. *J. Cell Biol.* **168**, 697–703 (2005).
37. Ling, S.-C., Fahrner, P. S., Greenough, W. T. & Gelfand, V. I. Transport of *Drosophila* fragile X mental retardation protein-containing ribonucleoprotein granules by kinesin-1 and cytoplasmic dynein. *Proc. Natl Acad. Sci. USA* **101**, 17428–17433 (2004).
38. Nan, X., Sims, P. A., Chen, P. & Xie, X. S. Observation of individual microtubule motor steps in living cells with endocytosed quantum dots. *J. Phys. Chem. B* **109**, 24220–24224 (2005).
39. Gross, S. P. *et al.* Interactions and regulation of molecular motors in *Xenopus* melanophores. *J. Cell Biol.* **156**, 855–865 (2002).
40. Karki, S. & Holzbaur, E. L. F. Affinity chromatography demonstrates a direct binding between cytoplasmic dynein and the dynactin complex. *J. Biol. Chem.* **270**, 28806–28811 (1995).